Journal of Alloys and Compounds 505 (2010) 163–167

Contents lists available at ScienceDirect

Journal of Alloys and Compounds

journal homepage: www.elsevier.com/locate/jallcom

Excellent catalytic and electrochemical properties of the mesoporous MnO_2 nanospheres/nanosheets

Jian-Hua Cheng[a], Guang Shao[b,*], Hui-Juan Yu[b], Jie-Jun Xu[a]

[a] Key Laboratory for Pollution Control and Ecological Restoration in Regions of Industrial Clusters, College of Environmental Science and Engineering, South China University of Technology, Guangzhou 510006, People's Republic of China
[b] School of Chemistry and Chemical Engineering, Sun Yat-Sen University, Guangzhou 510275, People's Republic of China

ARTICLE INFO

Article history:
Received 21 April 2010
Received in revised form 22 May 2010
Accepted 29 May 2010
Available online 11 June 2010

Keywords:
Oxide materials
Chemical synthesis
Catalysis
Electronic properties

ABSTRACT

In this paper, we report the successful synthesis of mesoporous MnO_2 nanospheres composed of nanosheets via a facile hydrothermal route without any template. The phase and morphology of the products were characterized by means of X-ray diffraction (XRD), scanning electron microscopy (SEM), and transmission electron microscopy (TEM). The reaction time played an important role in the formation of mesoporous MnO_2 nanospheres. The obtained nanospheres showed superior catalytic ability in the degradation reaction of an aqueous solution of Rhodamine B (RhB) in the presence of H_2O_2. Electrochemical measurements predicted that the mesoporous MnO_2 nanosphere-modified electrode showed good electrocatalytic properties for the reduction of H_2O_2 in alkaline medium, which might have wide application in electrochemical analysis.

1. Introduction

Over the past decade, nanomaterials with well-controlled size, morphology, and chemical composition have been the focus of scientific research, due to their unique chemical/physical properties and potential applications in electronics, photonics, chemical sensing, and biological imaging [1–6]. These materials have been successfully synthesized, offering great opportunities to investigate their novel electronic and optical properties for deep fundamental insights into materials science.

Among the various metal-oxide semiconductors, manganese oxide (MnO_2) has attracted much attention because of its particular physical and chemical properties and because it possesses great potential as a selective heterogeneous catalyst [7], an adsorbent [8], and an electrochemical supercapacitor [9]. Composite electrodes based on the MnO_2-modified carbon powder proved to be useful for detection of H_2O_2, ascorbic acid and nitrite ions [10]. Recently, much effort has gone into the investigation of MnO_2 nanostructures because of their promising applications in high performance nanodevices [11–13]. Compton and coworkers [14] have reported the α- and β-MnO_2 nanorods produced significantly lower limits of detection and greater sensitivity towards H_2O_2 than the MnO_2 microparticles, which was likely attributed to an increased surface area. But the different surface or structural energies of these α- and β-MnO_2 nanorods may also play a role as suggested by the slightly lower limit of detection found at the β-MnO_2 nanorods compared to the α-MnO_2 nanorods [14].

Until now, various nanostructures of MnO_2 have been synthesized by different methods. Suib and coworkers [15] reported a self-assembly synthesis of γ-MnO_2 mesoporous hollow nanospheres, which are composed of porous γ-MnO_2 hexagonal nanoflakes. Xie and coworkers [16] promoted a solution-based catalytic route to synthesize various α-MnO_2 hierarchical structures and β-MnO_2 nanorods. Wang and Li [17] synthesized 1D, nanostructured β-MnO_2 using a hydrothermal method and obtained single crystal nanorods in a small scale.

Mesoporous materials have attracted much attention for their potential application as catalysts, adsorbents and sensors, as well as nanoreactors for making other novel nanostructured materials. In addition, numerous preparation methods have been proposed, such as sol–gel techniques [18], hydrolysis [19], polyglycol-assisted routes [20], inorganic and organic templates [21], ultrasonic methods, [22] and co-precipitation [23].

In this paper, mesoporous α-MnO_2 nanospheres composed of nanosheets with average diameters of 800 nm were obtained through a simple hydrothermal route without any template. The optical and electrical properties of the α-MnO_2 nanomaterials were also investigated.

2. Experimental

2.1. Preparation of the mesoporous MnO_2 nanospheres

All chemicals used in the experiment were of analytical grade and were used without further purification. In a typical procedure, 0.1 g of $KMnO_4$ and 1.0 mL of 5% H_2SO_4 solution were added to 30 mL of deionized water under magnetic stirring

* Corresponding author. Tel.: +86 20 84110918; fax: +86 20 84110996.
E-mail address: shaog@mail.sysu.edu.cn (G. Shao).

0925-8388/$ – see front matter © 2010 Elsevier B.V. All rights reserved.
doi:10.1016/j.jallcom.2010.05.169

to form the precursor solution. The solution was transferred into a stainless steel autoclave (50 mL capacity) and kept at 160 °C for 10 h and then cooled to room temperature naturally. The resultant precipitate was collected, washed with distilled water, absolute ethanol, and acetone thoroughly, and finally dried under vacuum at 60 °C for 10 h.

2.2. Characterization of the as-prepared MnO_2 nanospheres

The phase and crystallography of the products were characterized by a Shimadzu XRD-6000 X-ray diffractometer equipped with Cu Kα radiation (λ = 0.15406 nm). A scanning rate of 0.05° s^{-1} was applied to record the pattern in the 2θ range of 10–80°. The scanning electron microscopy (SEM) images were taken with an S-4800 field emitting scanning electron microscopy (FESEM). Transmission electron microscopy (TEM) images were captured with a JEOL-2010 transmission electron microscope, using an accelerating voltage of 200 kV. Brunauer–Emmett–Teller (BET) nitrogen adsorption–desorption was measured by using Micrometrics ASAP-2020 accelerated surface area and porosimetry system.

The optical properties of the products were investigated by a UV–vis spectrophotometer (Shimadzu U-4100). A small amount of MnO_2 nanospheres was dispersed in ethanol for UV–vis absorbance spectroscopy measurement in the wavelength range between 200 and 800 nm.

2.3. Catalytic activity of the as-prepared mesoporous MnO_2 nanospheres

The catalytic experiment was carried out by adding 100 mg of prepared α-MnO_2 nanosphere catalyst to 100 mL of aqueous Rhodamine B (RhB) solution with an initial concentration of 10 mg/L. The suspension was magnetically stirred for an hour in darkness to establish an absorption/desorption equilibrium of RhB. Subsequently, 2 mL of 30% H_2O_2 solution were added and the mixture was allowed to react at room temperature under continuous stirring. At given intervals, 2 mL of the suspension were extracted and subsequently centrifuged at a rate of 9000 rpm for 5 min. UV–vis absorption spectra of the supernatant were then measured using a Shimadzu U-4100 UV–vis absorbance spectroscope.

2.4. Electrocatalytics of the mesoporous α-MnO_2 nanospheres

The electrochemical measurement was performed on a CHI 620B Electrochemical Workstation with a three-electrode system consisting of an Ag/AgCl reference electrode, a platinum wire as a counter electrode and a bare or modified glassy carbon electrode (GCE) as a work electrode, employing a scanning rate of 100 mV/s and a rest time of 2 s. Prior to the experiment, solutions were purged with nitrogen for 30 min to remove oxygen. The MnO_2/GCE used as a working electrode was fabricated as follows: mesoporous α-MnO_2 nanospheres (0.01 g) were added to 5 mL of *N*, *N*-dimethylformamide (DMF) under ultrasonic irradiation to get a MnO_2 suspension. GCE (Φ = 2 mm) was polished with 0.05 μm of alumina slurry and washed with 30% nitric acid, ethanol, and water in an ultrasonic bath for a few minutes. After washing with sonication, the GCE was coated with 10 μL of α-MnO_2 suspension, and dried at room temperature.

3. Results and discussion

The crystal structure and phase composition of the products were first characterized using X-ray powder diffraction (XRD). Fig. 1(curve a) shows the X-ray diffraction analysis of the as-prepared MnO_2 nanospheres. All peaks were indexed to a tetragonal α-MnO_2 single crystal structure [space group: I4/m (87)] (JCPDS card. No. 44-0141) with lattice constants of $a = 0.9782 \pm 0.0009$ nm and $c = 0.2871 \pm 0.0006$ nm. No peaks of any other phase were detected, which indicated the high purity and crystallinity of the final product.

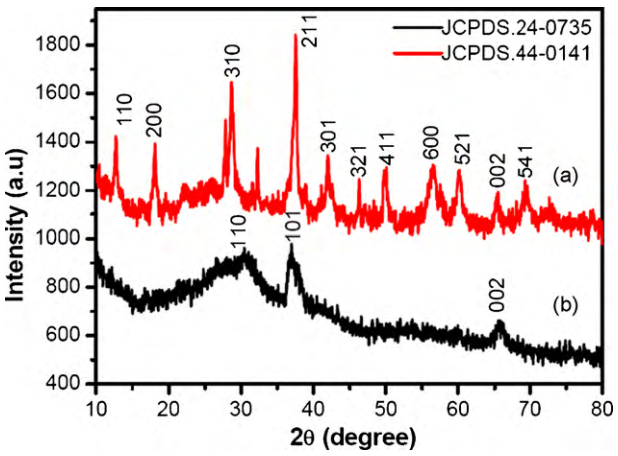

Fig. 1. (a) The XRD patterns of mesoporous α-MnO_2 nanospheres/nanosheets and (b) MnO_2 nanoparticles obtained for 2 h at 160 °C.

The morphology of the resulting sample was investigated by SEM. Fig. 2 shows the SEM images of the product prepared under hydrothermal reaction. The MnO_2 sample consisted of nanosphere/nanosheet nanostructures with about 90% ration (Fig. 2a). The nanospheres were uniform, with diameters of 800 nm. High-magnification SEM image (Fig. 2b) clearly revealed that the nanosheets in the corona were grown from the nanospheres in the core, and the surface of the nanosheet was very smooth.

Fig. 3 shows the TEM image of the prepared MnO_2 samples, revealing the nanosphere/nanosheet-like morphology features. Each nanosphere had a uniform width of 800 nm, which was confirmed by the SEM results.

To understand the growth process of the mesoporous α-MnO_2 nanospheres, a series of parallel experiments was performed and the results were checked with SEM. In the absence of H^+, with other conditions remaining unchanged, it was found that mesoporous MnO_2 nanospheres could not be obtained. From the experimental results, it was determined that the presence of an appropriate amount of H^+ played a crucial role in the growth of mesoporous α-MnO_2 nanospheres.

To understand the growth mechanism of the mesoporous MnO_2 nanospheres accurately, it was necessary to investigate the morphology evolution of the intermediates involved in the formation. Fig. 4a and b shows the SEM images of the products obtained after reaction for 2 and 5 h, respectively. After reaction for 2 h, the product was nanoparticles with diameters of 50–100 nm (Fig. 4a). Moreover, the XRD pattern (Fig. 1, curve b) could be assigned to metastable monoclinic β-MnO_2 (JCPDS card No. 24-

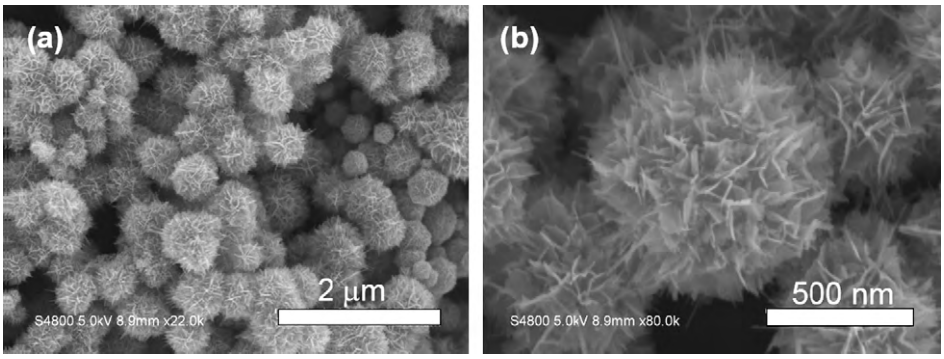

Fig. 2. SEM images of mesoporous α-MnO_2 with nanospheres/nanosheets morphology: (a) at low magnification, and (b) at high-magnification.

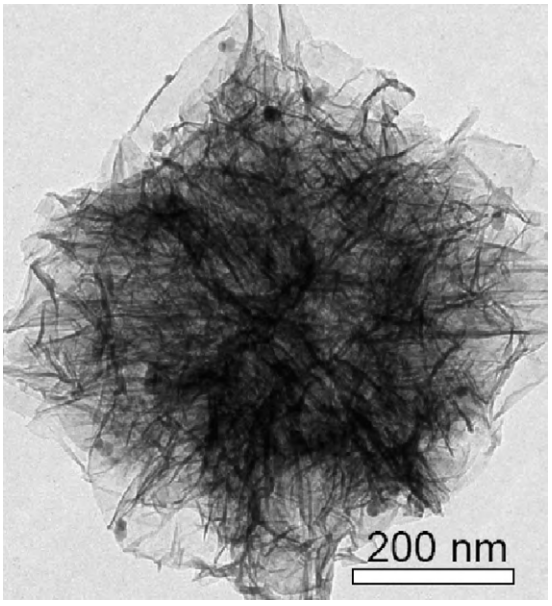

Fig. 3. TEM image of the mesoporous α-MnO_2 nanostructure.

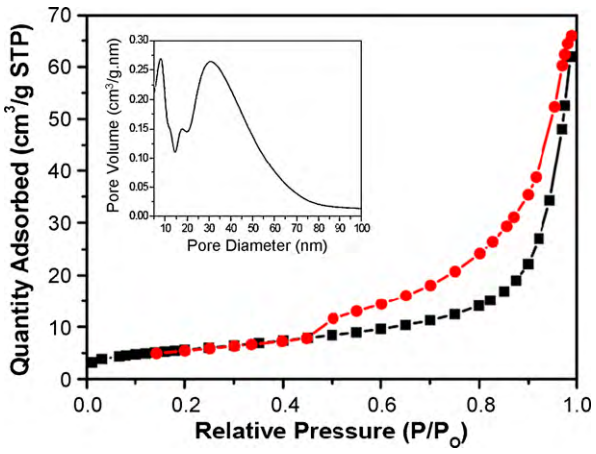

Fig. 5. N_2 adsorption–desorption isotherms and Barret–Joyner–Halenda (BJH) pore size distribution plots (inset) of the mesoporous α-MnO_2 nanostructure under hydrothermal reaction for 10 h.

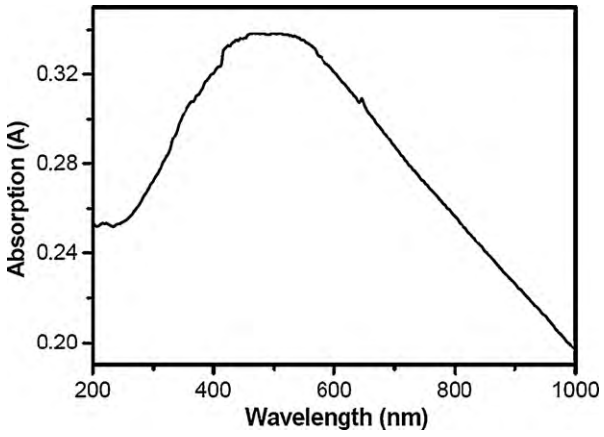

Fig. 6. UV–vis absorption spectrum of the mesoporous α-MnO_2 nanospheres/nanosheets.

0735). With an extension of the reaction time to 5 h, nanospheres were formed. As shown in Fig. 4b, nanosheets began to grow from the centers of the spheres. Eventually, the product evolved into pure nanospheres/nanosheets with uniform diameters of 800 nm (Fig. 2).

Based on the time-dependent experiments, we proposed the formation mechanism. At the beginning, the reaction produced β-MnO_2 nanoparticles directly. Under hydrothermal conditions, β-MnO_2 nanoparticles partially dissolved in the solution and generated free β-MnO_2 molecules. When the concentration of β-MnO_2 molecules was high enough, β-MnO_2 molecules recrystallized and formed crystalline α-MnO_2 molecule nuclei. These nuclei self-assembled to form nearly amorphous spheres. Afterward, the heterogeneous growth of nanosheets on the cores was exhibited by the intrinsic layered crystal structure. The formation mechanism was consistent with the previous report [24,25].

Such nanospheres/nanosheets possess a mesoporous structure, as evidenced by the nitrogen-sorption experiment (Fig. 5). The product of the mesoporous α-MnO_2 nanospheres had a wide, porous diameter distribution with a central pore-size distribution of *ca.* 36.2 nm, which was probably caused by the two kinds of porous architecture in the products: one within the microspheres and the other from the interspaces of the constituent nanoparticles. In addition, the surface area of the mesoporous α-MnO_2 was 20.2 m^2/g. Such mesoporous structure provides efficient transport pathways to their interior voids, which is critical for delivery, catalyst, and other applications.

Fig. 6 shows that the absorbance spectroscopy of the α-MnO_2 nanospheres exhibited prominent features at *ca.* 490 nm, slightly blue-shifted in comparison to the value of bulk MnO_2. As the optical property of materials can be modulated by changing the size and nanostructures, the α-MnO_2 nanospheres will be used in new

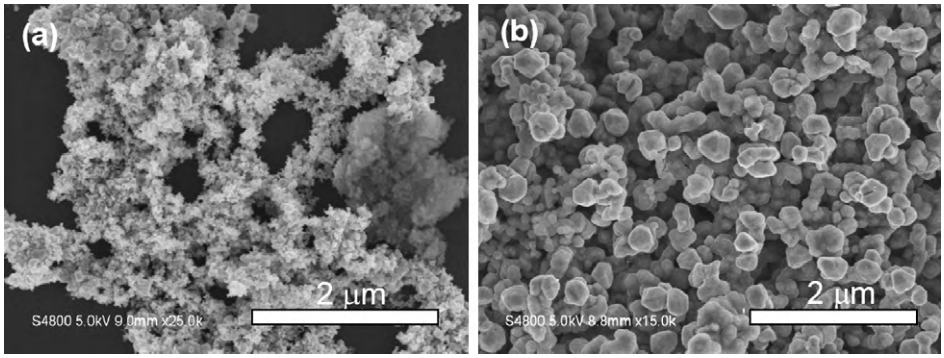

Fig. 4. SEM images of the samples prepared after hydrothermal reaction for (a) 2 h and (b) 5 h, showing the morphological evolution of the α-MnO_2 with nanospheres/nanosheets.

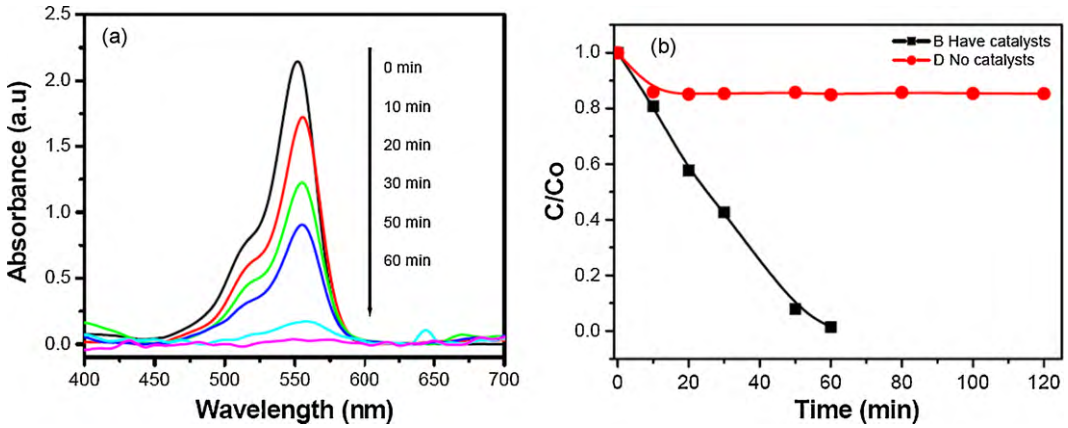

Fig. 7. (a) UV–vis spectral changes of RhB solution with reaction time in the presence of mesoporous α-MnO_2 nanospheres/nanosheets and (b) degradation of RhB using the as-prepared MnO_2 nanostructure as catalyst.

applications or to enhance the performance of currently existing devices.

3.1. The photocatalytic degradation property of mesoporous MnO_2 nanospheres

Previous work showed that metal semiconductors with certain morphology might be good catalysts for degradation of organic compounds. In order to investigate the catalytic property of the as-prepared α-MnO_2 nanospheres, we measured the optical property changes of some organic dyes, such as RhB. The characteristic absorption of RhB at $\lambda = 552$ nm was chosen to monitor the catalytic degradation process. Fig. 7a shows the absorption spectrum of an aqueous solution of RhB for various times. The absorption peak at $\lambda = 552$ nm diminished gradually as the visible light irradiation time increased, and completely disappeared after about an hour. No new absorption bands appeared in either the visible or the ultraviolet region. Fig. 7b (curve 1) shows that the relationship of $\ln C_{RhB}$ vs. reaction time is nearly linear, and the slope is 0.03571 ± 0.00211. So the reduction rate of RhB may be expressed as

$$r = 0.03571 C_{RhB}^2$$

For comparison, a contrast experiment was performed. In the absence of MnO_2 nanospheres, the peak intensity decreased only slightly. Fig. 7b (curve 2) shows the degradation of RhB with H_2O_2 (0.01 M) in the absence of catalyst. Even at high concentration, the degradation activity was slow. The above facts indicate that the as-prepared α-MnO_2 nanospheres/nanosheets have good catalytic degradation activity on some organic dyes.

A Fenton-like reaction is one of the effective advanced oxidation processes for wastewater treatment, and Fenton systems can only work efficiently under highly acidic conditions. This limits further application of traditional Fenton processes in wastewater treatment [26,27]. MnO_2 is able to act as a Fenton-like catalyst for H_2O_2 decomposition. From the above results, we found that the mesoporous α-MnO_2 nanospheres/nanosheets have a high Fenton oxidation activity on RhB at pH = 7.

As for the catalytic mechanism of the decomposition, the mesoporous α-MnO_2 nanospheres/nanosheets played an important role. Effective catalysts with an intermediate redox potential value of the donor–acceptor partner helped electron transfer and acted as an electron relay system [28]. Owing to the mesoporous nanosphere/nanosheet nanomaterials, the MnO_2 catalysts were provided with a large surface-to-volume ratio, which made the whole decomposition of RhB dye take place fast and effectively.

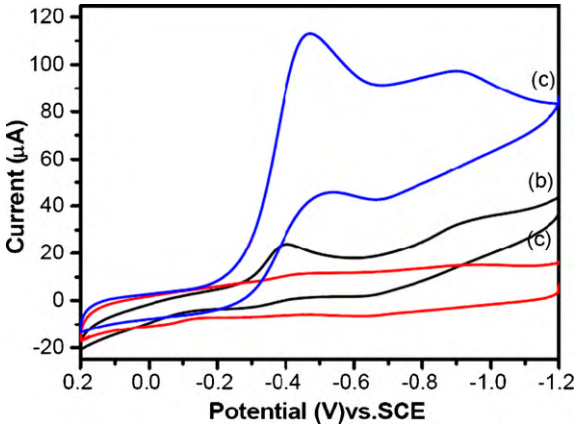

Fig. 8. CVs of H_2O_2 in 0.1 M NaOH solution with scan rate of 50 mV s^{-1}: (a) α-MnO_2/GCE, (b) bare GCE and 1 mM H_2O_2, and (c) α-MnO_2/GCE and 1 mM H_2O_2.

3.2. Electrochemical property of the mesoporous α-MnO_2 nanospheres/nanosheets

Cyclic voltammetry (CV) was performed to characterize the electrochemical behaviour of MnO_2 nanospheres. Fig. 8 shows the electrochemical response of MnO_2-modified electrodes to 1 mM of H_2O_2 in a 0.1 M NaOH solution. MnO_2 was electrochemically inactive in the basic solution (curve a). However, on adding H_2O_2 to the 0.1 M NaOH solution, two obvious cathodic peaks appeared at −0.46 and −0.92 V at the α-MnO_2-modified GCE in the forward scan, and another cathodic peak appeared at −0.53 V in the reverse scan (curve c). The observed voltammetric behaviour of solution phase redox couples at mesoporous α-MnO_2 nanospheres/nanosheets modified electrode surfaces reflects the thin layer finite diffusion effects [29–32]. Moreover, when the unmodified GCE was measured in 0.1 M NaOH solution containing 1 mM of H_2O_2 (curve b), the cathodic peak currents were low. This phenomenon implies that the as-prepared products could improve the electron transfer between H_2O_2 and the GCE. The mesoporous MnO_2 nanosphere/nanosheet structure could increase the number of active sites for adsorption, which would contribute to the high catalytic activity for the reduction of H_2O_2.

4. Conclusions

In summary, mesoporous α-MnO_2 nanosphere structures with diameters of *ca.* 800 nm were successfully synthesized under

hydrothermal conditions without any template. The reaction time might play a key role in the process of crystal growth. The as-prepared products exhibited superior catalytic activity for the degradation of RhB in the presence of H_2O_2, and the mesoporous α-MnO_2 nanostructures showed good electrocatalytic properties for the reduction of H_2O_2 in alkaline medium. The modified electrode was quite stable and had good reproducibility, which allows for wide applications in bioelectroanalysis, capillary electrophoresis, miniaturized total analysis systems, and other fields.

Acknowledgements

This work was supported by National S&T Major Project Foundation of China (No. 2008ZX07211005), the Natural Science Foundation of Guangdong Province (No. 8451027501001447), and the Research Fund for the Doctoral Program of Higher Education of China (No. 20090171120025).

References

[1] C.G. Hu, H. Liu, W.T. Dong, Y.Y. Zhang, G. Bao, C.S. Lao, Z.L. Wang, Adv. Mater. 19 (2007) 470–474.
[2] Z.W. Pan, Z.R. Dai, Z.L. Wang, Science 291 (2001) 1947–1949.
[3] J.S. Jie, W.J. Zhang, Y. Jiang, X.M. Meng, Y.Q. Li, S.T. Lee, Nano Lett. 6 (2006) 1887–1892.
[4] X.M. Han, B. Zhang, S.K. Guan, J.D. Liu, X. Zhang, R.F. Chen, J. Alloys Compd. 461 (2008) 26–28.
[5] W. Chen, N. Wang, L. Liu, Y.R. Cui, X. Cao, Q.J. Chen, L. Guo, Nanotechnology 20 (2009) 445601–445608.
[6] A.C. Yanes, A. Santana-Alonso, J. Mendez-Ramos, J. Del-Castillo, V.D. Rodriguez, J. Alloys Compd. 480 (2009) 706–710.
[7] J. Dong, Y.T. Li, L.J. Zhang, C.S. Liu, L. Zhuang, L.N. Sun, J.M. Zhou, J. Chem. Technol. Biotechnol. 84 (2009) 1848–1853.
[8] J.B. Fei, Y. Cui, X.H. Yan, W. Qi, Y. Yang, K.W. Wang, Q. He, J.B. Li, Adv. Mater. 20 (2008) 452–456.
[9] D.W. Liu, B.B. Garcia, Q.F. Zhang, Q. Guo, Y.H. Zhang, S. Sepehri, G.Z. Cao, Adv. Funct. Mater. 19 (2009) 1015–1023.
[10] B. Sljukic, R.G. Compton, Electroanalysis 19 (2007) 1275–1280.
[11] C.Z. Wu, W. Xie, M. Zhang, L.F. Bai, J.L. Yang, Y. Xie, Chem. Eur. J. 15 (2009) 492–500.
[12] S.B. Hocevar, B. Ogorevc, K. Schachl, K. Kalcher, Electroanalysis 16 (2004) 1711–1716.
[13] Y.J. Yang, E.H. Liu, L.M. Li, Z.Z. Huang, H.J. Shen, X.X. Xiang, J. Alloys Compd. 487 (2009) 564–567.
[14] C. Batchelor-McAuley, L.D. Shao, G.G. Wildgoose, M.L.H. Green, R.G. Compton, New J. Chem. 32 (2008) 1195–1203.
[15] Y.S. Ding, X.F. Shen, S. Gomez, H. Luo, M. Aindow, S.L. Suib, Adv. Funct. Mater. 16 (2006) 549–555.
[16] Z.Q. Li, Y. Ding, Y.J. Xiong, Q. Yang, Y. Xie, Chem. Commun. (2005) 918–920.
[17] X. Wang, Y.D. Li, J. Am. Chem. Soc. 124 (2002) 2880–2881.
[18] J. Bao, Z.L. Liu, Y. Zhang, N. Tsubaki, Catal. Commun. 9 (2008) 913–918.
[19] H. Li, H.L. Shi, H. Liang, X. Li, L. Li, M. Ruan, Mater. Lett. 62 (2008) 1410–1413.
[20] Y.Y. Xu, D.R. Chen, X.L. Jiao, K.Y. Xue, J. Phys. Chem. C 111 (2007) 16284–16289.
[21] H.R. Chen, X.P. Dong, J.L. Shi, J.J. Zhao, Z. Hua, J.H. Gao, M.L. Ruan, D.S. Yan, J. Mater. Chem. 17 (2007) 855–860.
[22] S.M. Zhu, H.S. Zhou, M. Hibino, I. Honma, M. Ichihara, Adv. Funct. Mater. 15 (2005) 381–386.
[23] Y.J. Zhang, Q.X. Hu, B. Hu, Z.Y. Fang, Y.T. Qian, Z.D. Zhang, Mater. Chem. Phys. 96 (2006) 16–21.
[24] W. Xiao, D.L. Wang, X.W. Lou, J. Phys. Chem. C 114 (2010) 1694–1700.
[25] X. Wang, Y.D. Li, Chem. Eur. J. 9 (2003) 300–306.
[26] Z.H. Ai, L.R. Lu, J.P. Li, L.Z. Zhang, J.R. Qiu, M.H. Wu, J. Phys. Chem. C 111 (2007) 4087–4093.
[27] Z.H. Ai, L.Z. Zhang, F.H. Kong, H. Liu, W.T. Xing, J.R. Qiu, Mater. Chem. Phys. 111 (2008) 162–167.
[28] N.R. Jana, Z.L. Wang, T. Pal, Langmuir 16 (2000) 2457–2463.
[29] L. Xiao, G.G. Wildgoose, R.G. Compton, Sens. Actuators B 138 (2009) 524–531.
[30] G.P. Keeley, M.E.G. Lyons, Int. J. Electrochem. Sci. 4 (2009) 794–809.
[31] I. Streeter, G.G. Wildgoose, L.D. Shao, R.G. Compton, Sens. Actuators B 133 (2008) 462–466.
[32] L. Xiao, G.G. Wildgoose, A. Crossley, R.G. Compton, Sens. Actuators B 138 (2009) 397–401.